Solar Phys (2011) 274:5–27
DOI 10.1007/s11207-011-9921-4



# The Whole Heliosphere Interval in the Context of a Long and Structured Solar Minimum: An Overview from Sun to Earth

**S.E. Gibson · G. de Toma · B. Emery · P. Riley · L. Zhao · Y. Elsworth · R.J. Leamon · J. Lei · S. McIntosh · R.A. Mewaldt · B.J. Thompson · D. Webb**

Received: 22 June 2011 / Accepted: 16 September 2011 / Published online: 21 December 2011


**Abstract** Throughout months of extremely low solar activity during the recent extended solar-cycle minimum, structural evolution continued to be observed from the Sun through the solar wind and to the Earth. In 2008, the presence of long-lived and large low-latitude

Invited Review.

The Sun–Earth Connection near Solar Minimum
Guest Editors: M.M. Bisi, B.A. Emery, and B.J. Thompson

S.E. Gibson (✉) · G. de Toma · B. Emery · L. Zhao · S. McIntosh
NCAR/HAO, Boulder, CO, USA
e-mail: sgibson@ucar.edu

G. de Toma
e-mail: detoma@ucar.edu

B. Emery
e-mail: emery@ucar.edu

L. Zhao
e-mail: lzh@ucar.edu

S. McIntosh
e-mail: mscott@ucar.edu

P. Riley
Predictive Science Inc., San Diego, CA, USA
e-mail: pete@predsci.com

Y. Elsworth
University of Birmingham, Birmingham, UK
e-mail: ype@bison.ph.bham.ac.uk

R.J. Leamon
Montana State University, Bozeman, MT, USA
e-mail: robert.j.leamon@nasa.gov

J. Lei
University of Science and Technology of China, Beijing, China
e-mail: leijh@ustc.edu.cn

coronal holes meant that geospace was periodically impacted by high-speed streams, even though solar irradiance, activity, and interplanetary magnetic fields had reached levels as low as, or lower than, observed in past minima. This time period, which includes the first Whole Heliosphere Interval (WHI 1: Carrington Rotation (CR) 2068), illustrates the effects of fast solar-wind streams on the Earth in an otherwise quiet heliosphere. By the end of 2008, sunspots and solar irradiance had reached their lowest levels for this minimum (*e.g.*, WHI 2: CR 2078), and continued solar magnetic-flux evolution had led to a flattening of the heliospheric current sheet and the decay of the low-latitude coronal holes and associated Earth-intersecting high-speed solar-wind streams. As the new solar cycle slowly began, solar-wind and geospace observables stayed low or continued to decline, reaching very low levels by June – July 2009. At this point (*e.g.*, WHI 3: CR 2085) the Sun–Earth system, taken as a whole, was at its quietest. In this article we present an overview of observations that span the period 2008 – 2009, with highlighted discussion of CRs 2068, 2078, and 2085. We show side-by-side observables from the Sun's interior through its surface and atmosphere, through the solar wind and heliosphere and to the Earth's space environment and upper atmosphere, and reference detailed studies of these various regimes within this topical issue and elsewhere.

## 1. Introduction

This article describes the evolution of the recent solar minimum from Sun to Earth, providing linkage and context for the articles published as part of this Topical Issue of *Solar Physics*: "The Sun–Earth Connection near Solar Minimum."

When was the minimum? The answer to this question depends entirely on the definition of "minimum". If it is a single point in time, it varies depending on the observable. For example, solar-wind quantities tend to minimize later than solar quantities (Cliver and Ling, 2011; Emery *et al.*, 2011). For solar irradiance, it depends on wavelength: in general, the visible and near-ultraviolet wavelengths have their minima later than the extreme ultraviolet (EUV) wavelengths by several months (T. Woods, private communication, 2011). In all wavelengths, the slope of intensity *vs.* time was very flat, so that the minimum point is very sensitive to the period chosen for averaging (White *et al.*, 2011).

It is therefore fairly common to refer to solar "minimum" as an extended time of low activity. However, there is no consensus as to what precisely that time period should be. Considering only the articles of this topical issue, the periods referred to as minimum range from a year or less (Jian, Russell, and Luhmann, 2011; Webb *et al.*, 2011; White *et al.*, 2011) to two years or more (Araujo Pradere *et al.*, 2011; Aschwanden, 2011; Cliver and Ling, 2011; de Toma, 2011; Emery *et al.*, 2011; Jackman and Arridge, 2011; Lepping *et al.*, 2011; Muller, Utz, and Hanslmeier, 2011; Zhao and Fisk, 2011). An objective criterion was used to define one of these longer periods by Emery *et al.* (2011), of

R.A. Mewaldt
California Institute of Technology, Pasadena, CA, USA
e-mail: mewaldt@srl.caltech.edu

B.J. Thompson
NASA/GSFC, Greenbelt, MD, USA
e-mail: barbara.j.thompson@nasa.gov

D. Webb
Boston College, Boston, MA, USA
e-mail: david.webb@bc.edu

smoothed monthly sunspot number less than 20 (2006 – 2010). An alternative was presented by Jian, Russell, and Luhmann (2011), who justified a shorter interval (July 2008 – June 2009) as encompassing the minima of all key solar and heliospheric quantities.

Our goal is to tell the story of this minimum in its full context, from Sun to Earth. For this, a period of one year is too short, as it does not allow illustration of how various observables reached their minimum. Some observables, in particular those pertaining to magnetic-flux emergence and solar eruptions, were at low levels even before 2008 and did not change greatly until 2010 (Figure 1). Others depended on solar open-flux and heliospheric morphology, and showed ongoing and strong evolution before reaching their ultimate minimum configuration (Figure 2).

To focus, we limit our description to two years: 2008 and 2009. We illustrate aspects of the ongoing evolution of the system via three solar rotations, which serve as snapshots. These are the three rotations chosen as part of the Whole Heliosphere Interval campaign: CR 2068: 20 March – 16 April 2008 (WHI 1; Figures 3, 4 and 5), CR 2078: 17 December 2008 – 12 January 2009 (WHI 2; Figures 7, 8 and 9), and CR 2085: 26 June – 22 July 2009 (WHI 3; Figures 10, 11 and 12). In Section 2 we will describe the first half of 2008 and WHI 1. In Section 3 we consider the ongoing evolution through 2008 and 2009, with highlighted discussion of WHI 2 and WHI 3. In Section 4 we will discuss implications from Sun to Earth of this very quiet minimum. In Section 5 we will present our conclusions.

## 2. A Deep Solar Minimum Begins

The heliosphere in the first half of 2008 was quiet in terms of solar activity, but complex in terms of magnetic morphology. A broad band (in latitude) of mixed fast and slow wind (Tokumaru *et al.*, 2009) was superposed on a quiet background in terms of irradiance and magnetic activity. Unlike the last minimum (*i.e.* 1996), the solar-wind speed at the Earth had periodic fast solar-wind streams (Gibson *et al.*, 2009). It was, however, also unlike prior declining phases of solar activity because of the low levels of irradiance, solar-wind magnetic field, and solar activity.

### 2.1. Flux Emergence Low

As Figure 1 illustrates, by the beginning of 2008 running averages of sunspot number and irradiance had reached levels at, or lower than, the last minimum (Gibson *et al.*, 2009; Woods *et al.*, 2009; Solomon *et al.*, 2010; Kopp and Lean, 2011; Haberreiter, 2011; Araujo Pradere *et al.*, 2011). Solar activity was low, and no X-class flare had been observed since December 2006 (Nitta, 2011). The CME rate closely followed the decline in SSN in amplitude and phase (Webb *et al.*, 2011). CME rates in early 2008 were low, but slightly higher than the last minimum, possibly in part due to instrumental variation affecting counting (Cremades, Mandrini, and Dasso, 2011). CME masses were already lower than last minimum (Vourlidas *et al.*, 2010). Polar fields measured at the solar surface had reached relatively constant (2005 – 2009) values that were weaker than prior minima (Sheeley, 2008; Kirk *et al.*, 2009; de Toma, 2011). The magnetic-field strength in the solar wind over the poles as measured by *Ulysses* was also weak relative to the prior minimum (Smith and Balogh, 2008).

The results of this low solar activity and radiative output were manifest in the near-Ecliptic wind and at the Earth. The interplanetary magnetic field (IMF) and solar-wind dynamic pressure and electric field were already lower than prior minima, although not yet at

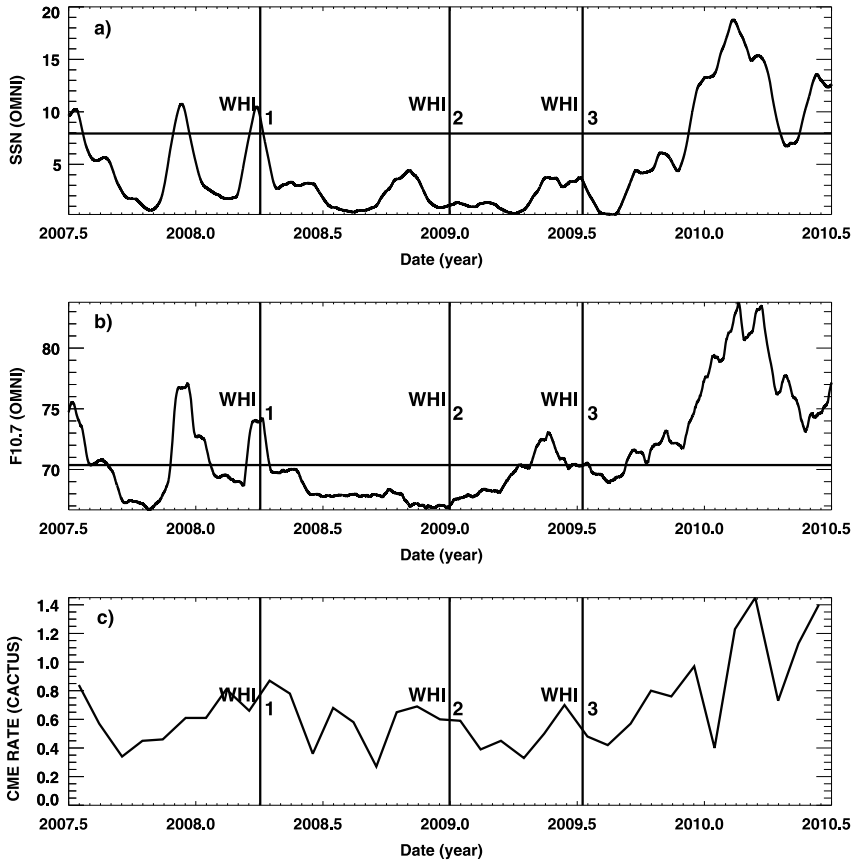


**Figure 1** Observables associated with magnetic-flux emergence. (a) Sunspot number (from OMNI database http://omniweb.gsfc.nasa.gov/). (b) Solar $F_{10.7}$ flux (solar flux units $10^{-22}$ W m$^{-2}$ Hz$^{-1}$ from OMNI database). (c) Solar activity (CME rate events day$^{-1}$ from automatic CACTus catalogue courtesy B. Bourgoignie (SIDC)). (a – b) are smoothed by a 27-day running average, (c) averaged over one month and corrected for duty cycle. By the beginning of 2008, these quantities had reached low levels – in the case of (a – b) lower than levels reached last minimum (horizontal lines – determined from 90-day running averages), and, notwithstanding some bumps (*e.g.* the active-region complex around WHI 1), they stayed at low levels until late in 2009.

their lowest point for this one (Emery *et al.*, 2011). The Earth's global-mean thermospheric density at 400 km had similarly dropped to levels lower than the previous minimum (Emmert, Lean, and Picone, 2010; Solomon *et al.*, 2010), and ionospheric total electron content (TEC) had reached levels by July 2007 that were comparable to those measured in July 2009 (Araujo Pradere *et al.*, 2011).

## 2.2. Open Flux Coherently Complex

Figure 2 demonstrates, however, that the distribution of open flux remained complex, with consequences throughout the heliosphere and at the Earth. The peculiarity of this period lay in the weak polar fields (Sheeley, 2008). Coronal structure was not dipolar: higher-order multipoles of magnetic field were significant. At this time there was also a large equatorial dipole component, which represented the longitudinal asymmetry that was present

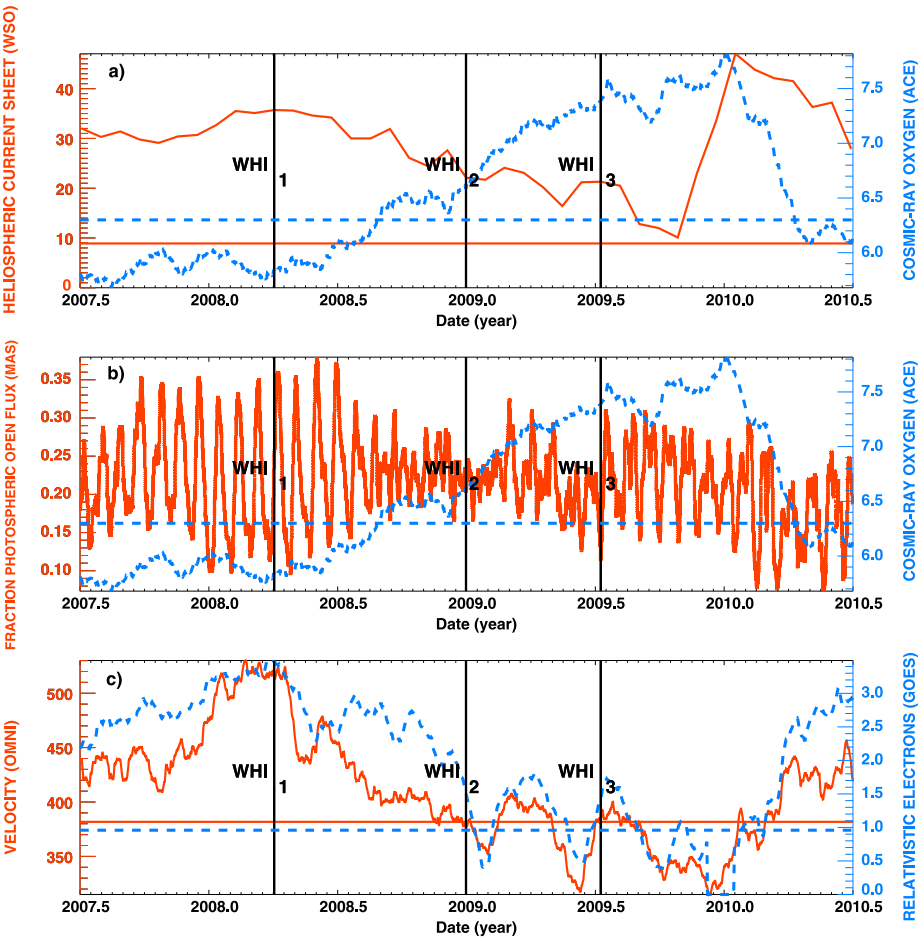


**Figure 2** Quantities associated with the evolution of open flux and heliospheric global morphology. Blue line: (a) and (b) ACE cosmic-ray oxygen intensity (176 – 238 MeV nucleon$^{-1}$). Red line: (a) Heliospheric current sheet (HCS) classic tilt from Wilcox Solar Observatory (degrees); (b) Coronal-hole fractional area calculated from Predictive Science Magnetohydrodynamics on a Sphere (MAS) modeled open magnetic–field-line footpoints at the central meridian *vs.* time (Riley *et al.*, 2011), showing periodic variation in the coronal-hole area for the first half of 2008. Note the MAS model uses a polar-field corrected SOHO/MDI boundary condition so that there is not seasonal variation. Blue line: (c) GOES > 2 MeV relativistic electron-number flux – particle flux units averaged over multiple satellites as described by Emery *et al.* (2011), and plotted on logarithmic scale. Red line: (c) Solar-wind velocity at the Earth (OMNI database (km s$^{-1}$). All are 27-day averages except the coronal-hole area in (b) which is seven-day averaged. These quantities had not reached levels equivalent to last minimum (horizontal lines – determined from 90-day running averages) by the beginning of 2008, and showed ongoing evolution throughout 2008 and 2009.

throughout much of 2008 (Abramenko *et al.*, 2010; Petrie, Canou, and Amari, 2011; Webb *et al.*, 2011). Low-latitude open-flux regions and associated coronal holes remained large and localized in longitude, and thus periodically recurring, for months after flux emergence stopped. The areas of low-latitude coronal holes are directly related to solar-wind speed and duration (L. Krista, private communication, 2011). Consequently, solar-wind high-speed streams (HSS) from these coronal holes periodically drove geomagnetic ac-

tivity and upper-atmosphere disturbances (Gibson *et al.*, 2009; Abramenko *et al.*, 2010; de Toma, 2011). Heliospheric current sheet (HCS) tilt also stayed elevated through the first half of 2008, unlike prior minima where it reached minimum values around the same time as sunspot number (Riley *et al.*, 2011).

Consequently, at the Earth, declining-phase-type periodic behavior was seen through much of 2008. Solar-wind speed and radiation-belt population were still elevated at the Earth for the first half of 2008, as compared to their eventual minimum levels. Cosmic rays similarly were not yet at their ultimate extrema (Mewaldt *et al.*, 2010) and exhibited periodic behavior (McIntosh *et al.*, 2011a).

### 2.3. Whole Heliosphere Interval (WHI 1)

The Whole Heliosphere Interval (WHI 1) was an internationally coordinated observing and modeling effort to characterize the heliosphere associated with one solar rotation (CR 2068). Many of the articles in this topical issue focus on WHI 1, and Thompson *et al.* (2011) provides a comprehensive description of the end-to-end observations obtained. WHI 1 was fairly typical of the first half of 2008, so we briefly summarize its features now and illustrate them with Figures 3, 4 and 5.

For roughly half the WHI 1 rotation the Sun was sunspot free, and irradiance was as low as any time this minimum. Indeed, a solar-minimum solar irradiance reference spectrum (SIRS) from 0.1 nm to 2400 nm was established from the WHI 1 "quiet side" using a combination of spacecraft and sounding-rocket observations (Chamberlin *et al.*, 2009; Woods *et al.*, 2009).

WHI 1 had an active side as well, however, as three active regions emerged that were the source of a temporary peak in CMEs and flares (Nitta, 2011; Petrie, Canou, and Amari, 2011; Webb *et al.*, 2011; Welsch, Christe, and McTiernan, 2011). These active regions were not long-lived, and largely dispersed within one or two solar rotations. Figure 3 shows them in the Carrington map (longitude *vs.* latitude) for the WHI 1 rotation. Also seen are the large, long-lived, and low-latitude coronal holes that were present for many months in 2008, and particularly clear during WHI 1. These included a northward extension of the southern-polar coronal hole between $120-180^\circ$ longitude and a near-equatorial coronal hole around $275^\circ$ longitude.

Figure 4 shows snapshots of the coronal magnetic field during WHI 1, and low-latitude open flux associated with these coronal holes can be seen on both sides in (a) and on the right-hand side in (b). Also present are unipolar, or "pseudo"-streamers: closed-field regions not associated with the HCS (Hundhausen, 1972; Zhao and Webb, 2002; Wang, Sheeley, and Rich, 2007). They are evident in magnetic-field-line plots as closed-field regions that lie between open field of the same polarity, and examples are indicated in Figure 4 with arrows (see also the discussion in Petrie, Canou, and Amari, 2011 and Riley *et al.*, 2011). Pseudo-streamers are a natural consequence of low-latitude coronal holes, and were accordingly common for this minimum.

The low-latitude open flux present during WHI 1 connected directly to the Earth. The colored symbols and lines overlaid on Figure 3 show the "footpoints" of field lines connecting the Earth to the Sun, and the projected path down to these footpoints from a source surface ($r = 2.5R_\odot$) at which the field is assumed to become radial. The color-coding in Figure 3(a) demonstrates the source of the fast wind in coronal holes, and of slow wind at the HCS or streamer-belt crossings, the most obvious of which occurring at a longitude of $240^\circ$. As expected (*e.g.* Zhao and Fisk, 2011), the "frozen-in" temperature at the source of these HSS as deduced from the oxygen-ion ratio is hot at this streamer-belt crossing and relatively cool in the HSS (Figure 3(b)).

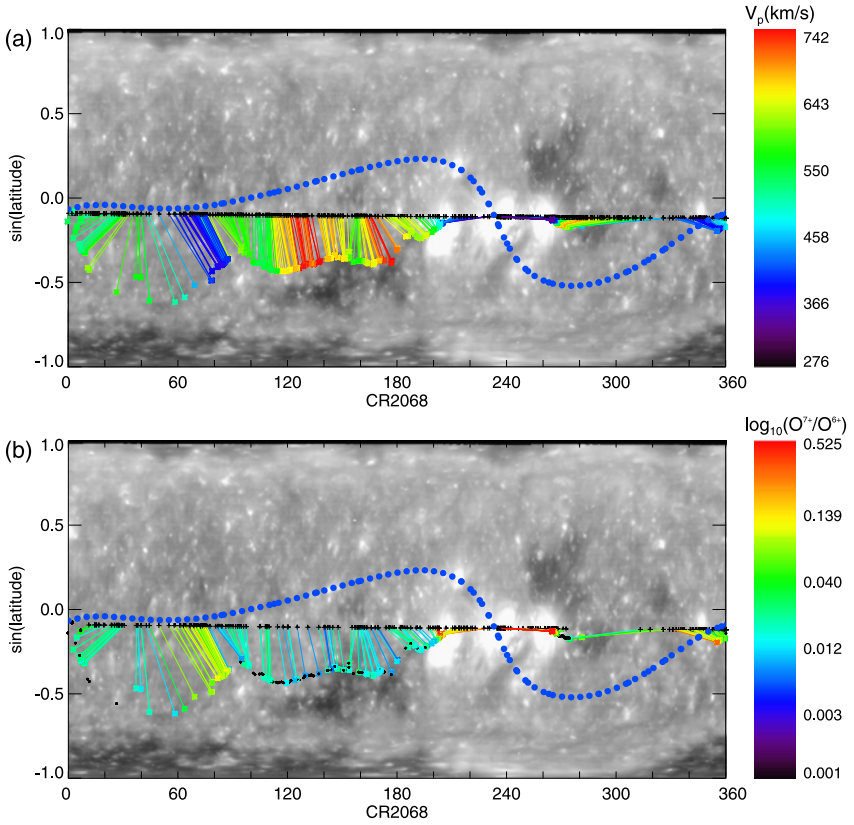


**Figure 3** WHI 1 (CR 2068: 20 March – 16 April 2008) rotation. SOHO/*Extreme Ultraviolet Imaging Telescope* (EIT) Carrington map, with overlaid sub-Earth field lines. Field lines are calculated by ballistically mapping back along a radial trajectory from the ACE spacecraft at 1 AU to the solar source surface ($r = 2.5 R_{\odot}$) using wind velocities measured at ACE, and then following the field line to the solar surface using a potential-field-source-surface (PFSS) extrapolation. Field lines are represented as a straight line between the coordinates (latitude, longitude) of their footpoints on the solar disk (small asterisks) and the coordinates (latitude, longitude) of the other end of the field line at the source surface (black "+" symbols). Blue dots represent neutral line (HCS) at the source surface. Color-coding represents (a) solar-wind velocity, and (b) solar-wind oxygen ratio (indicates temperature at source). Black asterisks (and no colored line drawn) on (b) indicate no oxygen composition data available.

Figure 5(a) shows the solar-wind velocity and magnetic-field strength at the Earth, and the two fast-wind streams associated with the two main coronal holes are clearly evident. Also shown is thermospheric density, illustrating how the fast-wind streams drive enhancements in the Earth's neutral upper atmosphere.

The Sun–Earth connecting field lines shown in Figure 3 were determined using a potential-field source-surface (PFSS) extrapolation of a SOHO/MDI photospheric magnetogram. There are a number of model-dependent factors that are known to affect the distribution of open *vs.* closed magnetic flux in photospheric-field extrapolations (*e.g.* Poduval and Zhao, 2004 and Lee *et al.*, 2011). Temporal evolution may also affect the accuracy of the models, which assume time-invariance of the photospheric boundary. Perhaps most important, however, may be the issue of polar magnetic fields. Due to line-of-sight projection, these are poorly resolved, and are generally reconstructed by incorporating some sort of

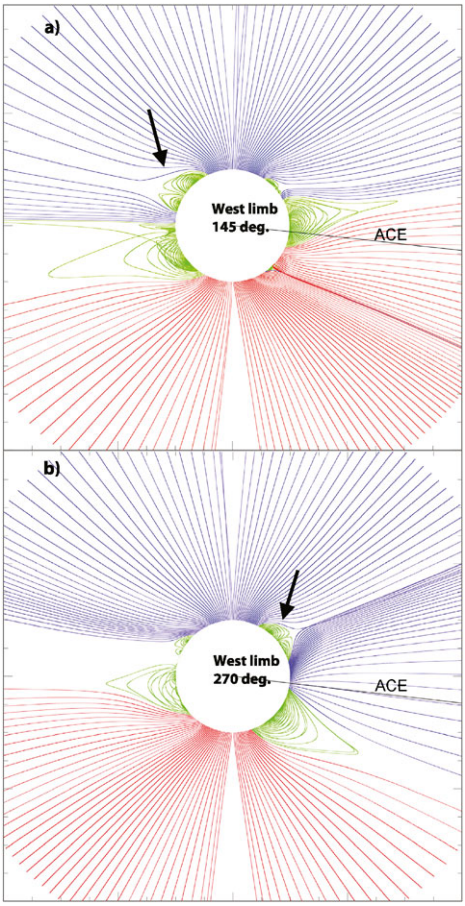


**Figure 4** (a – b) Snapshots of magnetic-field structure at different times/central meridian locations during WHI 1 (CR 2068: 20 March – 16 April 2008) from MAS numerical simulation. Blue represents negative open magnetic-field lines, and red positive open magnetic-field lines. Green are closed magnetic-field lines. Latitude of ACE spacecraft is shown: note that these images therefore represent a view orthogonal to the Sun–Earth line. Longitudes of west (right) limb for these images are indicated, corresponding to features seen at the central meridian by the Earth (thus structures there can be compared to those longitudes on the Carrington maps in Figure 3). Arrows indicate pseudo-streamers.

correction (Arge and Pizzo, 2000). We have used the default magnetic-field datacube in the SolarSoft PFSS software (Schrijver and DeRosa, 2003). To test the validity of this mapping, we can compare the direction of field lines – *i.e.*, whether they point outward from the Sun (positive) or inward to the Sun (negative) at their source at the solar photosphere as well as at their other end at 1 AU. Figure 5(b) shows this, and demonstrates that for WHI 1 the polarities are largely consistent.

## 2.4. Periodic Behavior

The near-equatorial, northern-polarity coronal hole survived for months (Abramenko *et al.*, 2010) and was an ongoing source of periodic solar-wind streams. Figure 6 illustrates this for the first half of 2008. We have removed seasonal variation via a PFSS extrapolation in which we do not map back from the Earth's heliolatitude, but rather trace field lines that intersect the solar equatorial plane at the source surface back to their footpoints at the photosphere (Leamon and McIntosh, 2009). The blue dots show these sub-equatorial footpoint latitudes and longitudes, and the red lines show the solar-wind velocity measured *in situ* (ballistically mapped back to the solar-wind source times).

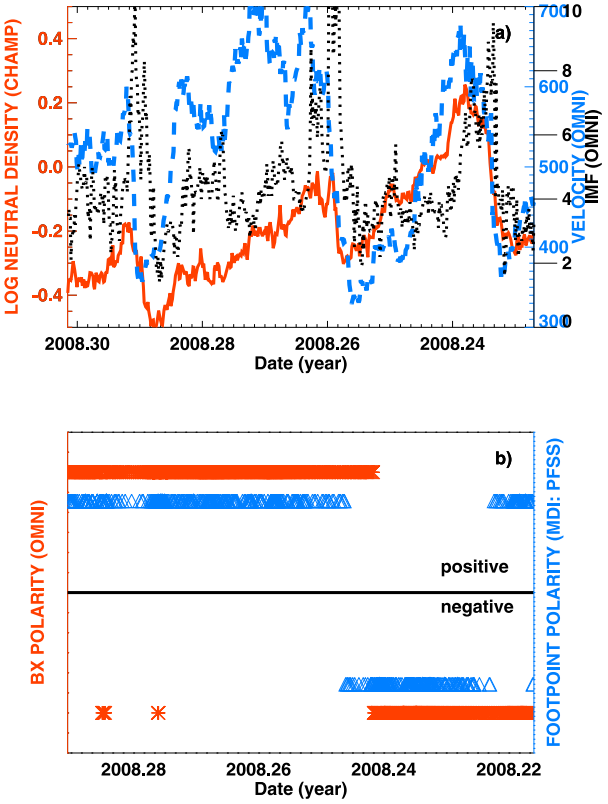


**Figure 5** WHI 1(CR 2068: 20 March – 16 April 2008) time series. (a) (Blue) OMNI solar-wind velocity and (black) interplanetary magnetic field (IMF), and (red) thermospheric neutral density (ascending orbit) from CHAMP satellite ($10^{-12}$ kg m$^{-3}$), illustrating the HSS and associated IMF spikes with corresponding thermospheric enhancements (*e.g.* Lei *et al.*, 2011). Quantities are plotted *vs.* the time they were measured, however, the interval shown is shifted to four days later than the WHI 1 solar interval to account for average solar-wind travel time. Note also that time goes opposite to the direction of longitude, and so has been plotted backward for ease of comparison to Figure 3. (b) (Red asterisks) Polarity of radial (outward from Sun = positive) component of magnetic field determined from OMNI $B_x$ (daily averages). (Blue triangles) Polarity of radial magnetic field at footpoint of Sun–Earth connecting field line (as described in Figure 3). OMNI $B_x$ measurements are plotted *vs.* time of solar-wind origin, assuming travel time based on solar-wind velocity measured *in situ* at the same time as $B_x$. The first HSS is rooted in the northern hemisphere, which had negative polarity, and the second in the southern hemisphere, with positive polarity. Time goes right to left.

A clear repeating pattern is seen. A near-equatorial source appears in rotation after rotation ranging from longitudes 250 – 300°. This was the source of corotating interaction regions (CIRs), where fast wind from the compact low-latitude coronal hole interacted with slow wind originating in the vicinity of the HCS. The HCS crossing is apparent as a discontinuity in longitude. After this, there is a more gradual stepping of field-line footpoints in longitude, and a second, broader fast-wind source occurs associated with the northern extension of the southern coronal hole. This repeated pattern led to ongoing solar-wind periodicities at the solar rotation and its harmonics (Emery *et al.*, 2011), and CIRs possessing large-amplitude Alfvénic fluctuations and driving periodic auroral, radiation-belt, ionospheric, and thermospheric enhancements for the months around WHI 1 (Gibson *et al.*, 2009; Lei *et al.*, 2011; Echer *et al.*, 2011; Wang *et al.*, 2011).

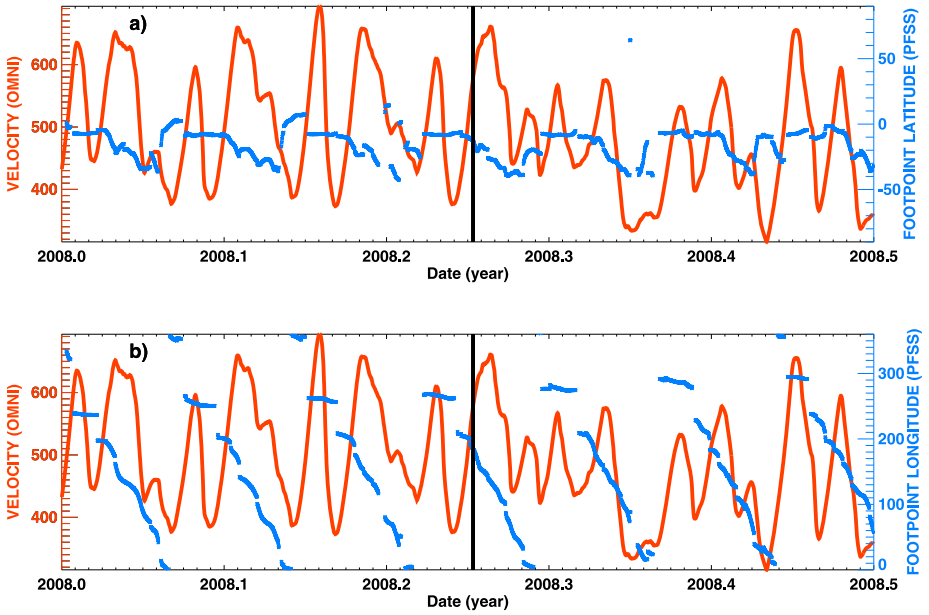


**Figure 6** (Blue) latitudes (a) and longitudes (b) of footpoints for field lines connecting to the solar Equator at the source surface (96-minute intervals) for a PFSS extrapolation of photospheric magnetic field (MDI) (*e.g.* Leamon and McIntosh, 2009). (Red) OMNI solar-wind velocities (seven-day running averaged). Vertical line shows the center of WHI 1. This demonstrates the persistence of a near-equatorial wind stream source at around 250 – 300° longitude, and the periodic behavior (two – three per rotation) of solar-wind streams during the first half of 2008.

## 3. A Long Minimum Continues to Evolve

Regardless of whether one prefers to consider the initial WHI 1 campaign as a peculiar declining phase or a peculiar minimum phase, it is clear that it does not, on its own, typify the extended minimum. We now discuss the evolution after WHI 1, and the routes to minimum of various solar, heliospheric, geospace, and atmospheric quantities.

### 3.1. WHI 2: Descending into the Depths

#### *3.1.1. Open Flux Loses Coherence*

From mid-2008 to 2009, the low-latitude coronal hole fragmented, so that open flux was no longer localized in large and coherent regions (de Toma, 2011; Petrie, Canou, and Amari, 2011). This was clearly seen in Figure 2(b), as the envelope of open-flux area variation decreases sharply starting in mid-2008, and becomes aperiodic by 2009. The rotational signal in radiative output also lost periodic behavior at this time, as the last vestiges of active regions at the "active longitudes" faded away (White *et al.*, 2011).

Figure 7 shows a Carrington map of our second focus period, WHI 2, (CR 2078: 17 December 2008 – 12 January 2009). Low-latitude coronal holes were still present, and Figure 8 shows that open flux was poking out from many latitudes. However, these coronal holes were not as large or as localized longitudinally as earlier in 2008, with consequences for the solar wind at Earth and resulting modulation of geospace and atmospheric quantities. Figure 9(a) shows that, although fast-wind streams were still present at the time of WHI 2, they

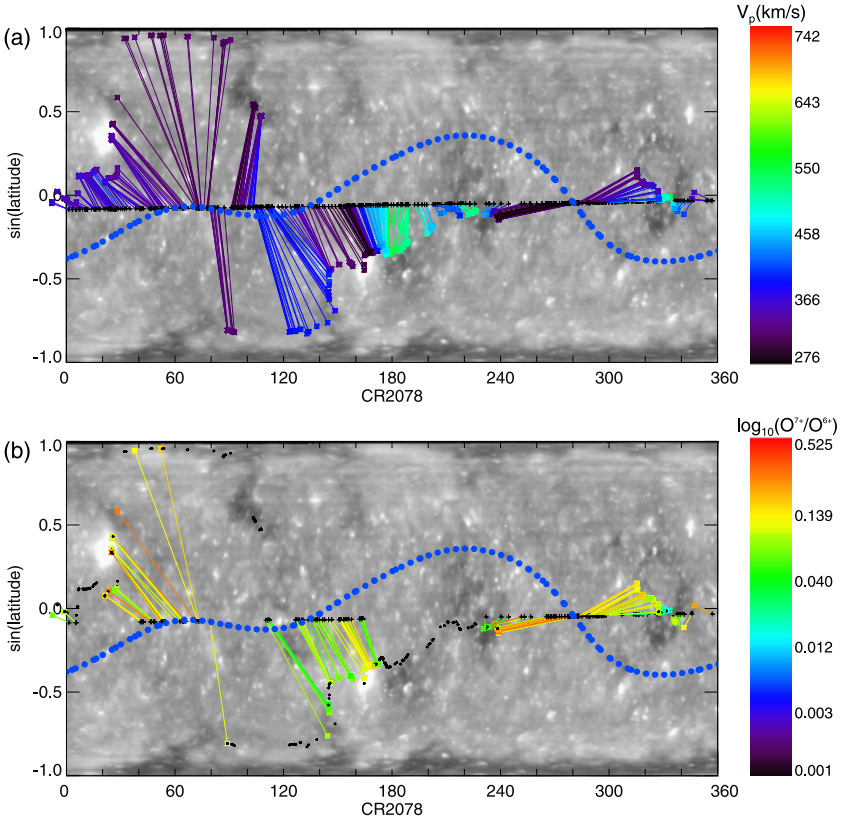


**Figure 7** WHI 2 (CR 2078: 17 December 2008 – 12 January 2009) rotation. SOHO/EIT Carrington map, with overlaid sub-Earth field lines. Field lines are calculated by ballistically mapping back along a radial trajectory from the ACE spacecraft at 1 AU to the solar source surface ($r = 2.5R_{\odot}$) using wind velocities measured at ACE, and then following the field line to the solar surface using a potential-field-source-surface (PFSS) extrapolation. Field lines are represented as a straight line between the coordinates (latitude, longitude) of their footpoints on the solar disk (small asterisks) and the coordinates (latitude, longitude) of the other end of the field line at the source surface (black "+" symbols). Blue dots represent the neutral line (HCS) at the source surface. Color-coding represents (a) solar-wind velocity, and (b) solar-wind oxygen ratio (indicates temperature at source). Black asterisks (and no colored line drawn) on (b) indicate no oxygen composition data available.

were shorter and less strong. Thermospheric density overall was very low during WHI 2, so response to these fast-wind streams stands out against the low background (seasonal differences must also be considered in comparing WHI 1 and WHI 2). Nevertheless, these fast-wind streams were not periodic: Lomb–Scargle analysis of solar-wind velocity (Emery *et al.*, 2011) showed that the solar-rotation harmonics decreased in the months after WHI 1, reaching low levels around WHI 2 (see also Jian, Russell, and Luhmann, 2011).

The average velocity decreased sharply as periodic HSS stopped dominating the solar wind at Earth (Emery *et al.*, 2011; Cliver and Ling, 2011). Radiation-belt populations also subsequently diminished (Russell, Luhmann, and Jian, 2010), and the HCS flattened as a result of axisymmetry. Lower-velocity, flattening HCS, and ongoing decrease in IMF all contributed to a climb in cosmic rays (Mewaldt *et al.*, 2010).

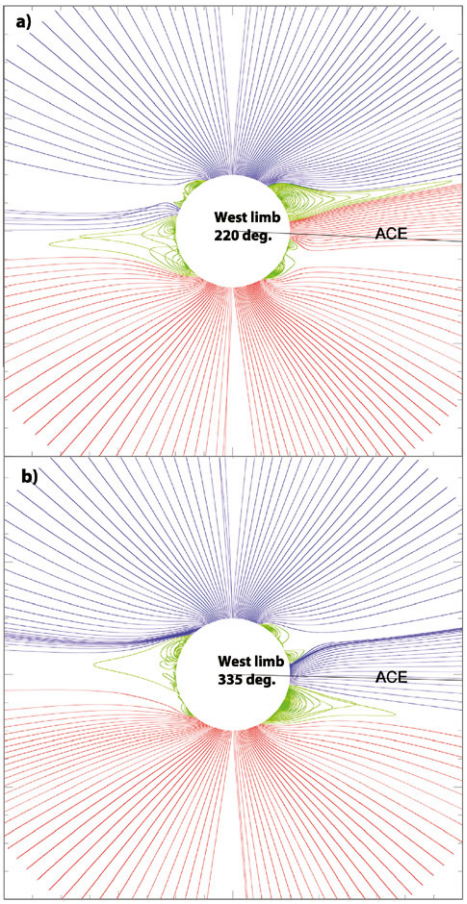


**Figure 8** (a – b) Snapshots of magnetic-field structure at different times/central meridian locations during WHI 2 (CR 2078: 17 December 2008 – 12 January 2009) from MAS numerical simulation. Blue represents negative open magnetic-field lines, and red positive open magnetic-field lines. Green are closed magnetic-field lines. Latitude of ACE spacecraft is shown: note that these images therefore represent a view orthogonal to the Sun–Earth line. Longitudes of west (right) limb for these images are indicated, corresponding to features seen at the central meridian by the Earth (thus structures there can be compared to those longitudes on the Carrington maps in Figure 7).

### *3.1.2. Closed-Field Complexity*

Despite the flattening of the HCS, the magnetic morphology of the coronal field was still complex. Because the open flux was weak and non-dipolar, it did not expand strongly, confining streamers to the Equator. This had been evident during WHI 1, and Cremades, Mandrini, and Dasso (2011) pointed out that trajectories of CMEs were not deflected to low latitudes as they had been in 1996 when the field was more dipolar. Later in 2008 and 2009 the polar dipole field remained relatively weak compared to higher-order multipoles of the field, so closed magnetic structures and associated streamers occupied a wide band of latitudes (Judge *et al.*, 2010). Indeed, Vasquez *et al.* (2011) found that the total closed-field volume was higher for WHI 2 than WHI 1, which they interpreted as due to high gas pressure in the streamers relative to surrounding open field.

Pseudo-streamers were still evident during WHI 2 (Figure 8). Thus, although the "streamer belt" as seen in the corona occupied a wide band of latitudes, it was a superposition of smaller closed-field structures. The central closed-field streamer associated with the flattening, now largely equatorial HCS occupied only part of the wide band of closed field that characterized this minimum.

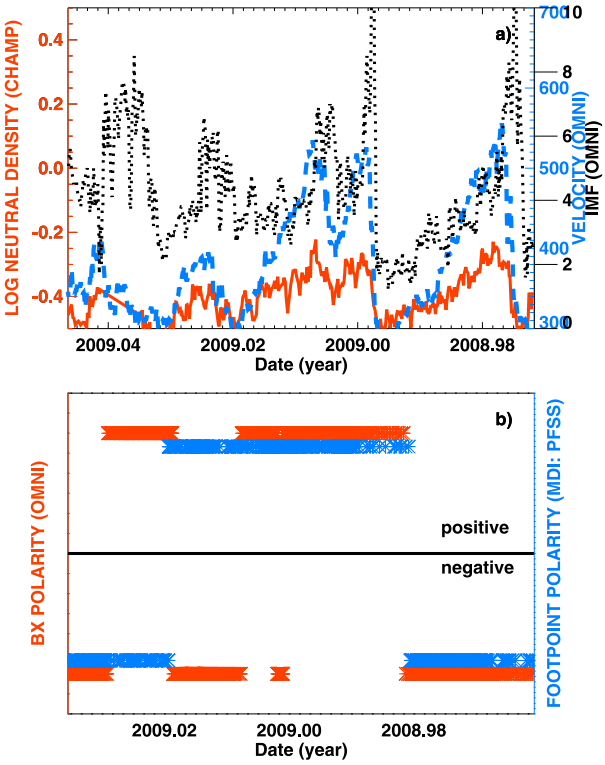


**Figure 9** WHI 2 (CR 2078: 17 December 2008 – 12 January 2009) time series. (a) (Blue) OMNI solar-wind velocity and (black) interplanetary magnetic field (IMF), and (red) thermospheric neutral density (ascending orbit) from CHAMP satellite ($10^{-12}$ kg m$^{-3}$). Quantities are plotted *vs.* the time they were measured, however, the interval shown is shifted to four days later than the WHI 2 solar interval to account for average solar-wind travel time. Note also that time goes opposite to the direction of longitude, and so has been plotted backward for ease of comparison to Figure 7. (b) (Red asterisks) Polarity of radial (outward from Sun = positive) component of magnetic field determined from OMNI $B_x$ (daily averages). (Blue triangles) Polarity of radial magnetic field at footpoint of Sun–Earth connecting field line (as described in Figure 7). OMNI $B_x$ measurements are plotted *vs.* time of solar-wind origin, assuming travel time based on solar-wind velocity measured *in situ* at the same time as $B_x$. Time goes right to left.

This provides insight into the result of Zhao and Fisk (2011): that hot material (as demonstrated by high $O^{7+}/O^{6+}$ composition) in the slow solar wind occupied a narrower band about the HCS for this minimum as opposed to the last, while slow wind in general occupied a wider band. The large band of slow wind may have its source at the boundaries of all closed-field regions, including pseudo-streamers, as supported by *in-situ* measurements of unipolar stream signatures in the slow wind (Riley *et al.*, 2011; Riley and Luhmann, 2011). However, Zhao and Fisk (2011) argue that only the HCS-associated "streamer stalk" would yield the narrower band of hot, slow wind.

Figure 9(b) compares polarity between the PFSS model Sun–Earth field-line footpoints and that measured in the solar wind for WHI 2. The agreement is reasonably good, although late in the month (and so lower Carrington rotation longitudes) the agreement is less consistent. The HCS is quite flat here, so that small perturbations lead to jumps in connectivity from North to South.

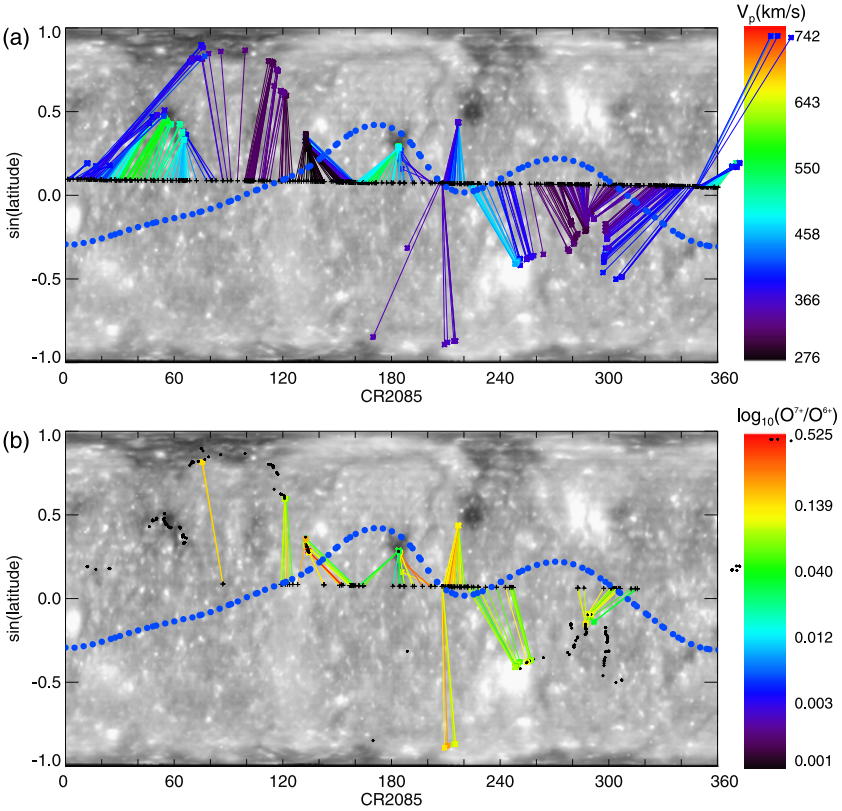


**Figure 10** WHI 3 (CR 2085: 26 June – 22 July 2009) rotation. SOHO/EIT Carrington map, with overlaid sub-Earth field lines. Field lines are calculated by ballistically mapping back along a radial trajectory from the ACE spacecraft at 1 AU to the solar source surface ($r = 2.5 R_\odot$) using wind velocities measured at ACE, and then following the field line to the solar surface using a potential-field-source-surface (PFSS) extrapolation. Field lines are represented as a straight line between the coordinates (latitude, longitude) of their footpoints on the solar disk (small asterisks) and the coordinates (latitude, longitude) of the other end of the field line at the source surface (black "+" symbols). Blue dots represent the neutral line (HCS) at the source surface. Color-coding represents (a) solar-wind velocity, (b) solar-wind oxygen ratio (indicates temperature at source). Black asterisks (and no colored line drawn) on (b) indicate no oxygen composition data available.

### 3.2. WHI 3: The Porcupine Sun

Our final period of focus (WHI 3) occurred at a time when properties in the heliosphere had evolved nearly to their ultimate minimum states and yet solar irradiance and activity were still low. It was a time when the system was quiet from Sun to Earth.

For the first half of 2009, between WHI 2 and WHI 3, the emergence and subsequent evolution of a new-cycle flux at mid latitudes resulted in the formation of short-lived small coronal holes (Wang and Robbrecht, 2011; de Toma, 2011), particularly in the North. These coronal holes are seen in Figure 10, which indicates that many of the Earth-connecting field lines originate in them. The open-flux regions at mid-to-low latitudes are also evident in Figure 11.

Figure 12(a) shows an overall weakness and lack of coherence in the solar-wind velocity and magnetic field during this rotation. It has been argued that the mid-latitude placement of

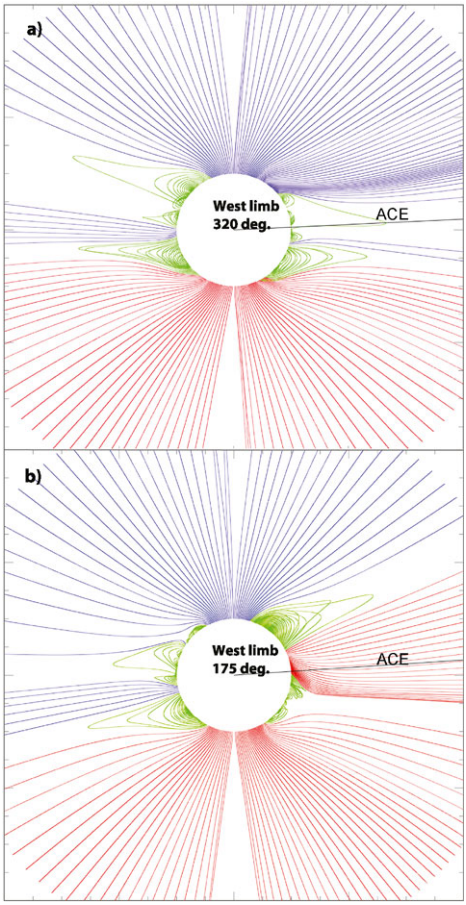


**Figure 11** (a – b) Snapshots of magnetic-field structure at different times/central meridian locations during WHI 3 (CR 2085: 26 June – 22 July 2009) from MAS numerical simulation. Blue represents negative open magnetic-field lines, and red positive open magnetic-field lines. Green are closed magnetic-field lines. Latitude of ACE spacecraft is shown: note that these images therefore represent a view orthogonal to the Sun–Earth line. Longitudes of west (right) limb for these images are indicated, corresponding to features seen at the central meridian by the Earth (thus structures there can be compared to those longitudes on the Carrington maps in Figure 10).

small coronal holes was a direct cause of the weakness of the IMF as well as the solar-wind magnetic variance (Tsurutani, Echer, and Gonzalez, 2011). The difference between WHI 1 and WHI 3 illustrates this point nicely. In the former the sources of the Earth-intersecting solar wind were largely restricted to the equatorial coronal hole and the southern-polar hole and its extension. In WHI 3, the Sun-to-Earth connection danced from source to source. The discrepancy between model and observed polarities in Figure 12(b) means that at least one of those footpoint sources may be misrepresented on Figure 10; however, we believe the qualitative nature of the global magnetic morphology is well captured. The MAS MHD model of Figure 11 is consistent with it, indicating an overall trend from WHI 1 to WHI 3 toward smaller scales of both open- and closed-flux regions. The global magnetic morphology at the bottom of this minimum was akin to a porcupine, with small-scale structures poking out all over.

## 4. Discussion: A Minimum's Minimum?

### 4.1. Flux Churning and Local Dynamo

The drive toward smaller spatial scales for solar magnetic structures may be the result of ongoing diffusion of the solar-surface magnetic field in the absence of significant new flux

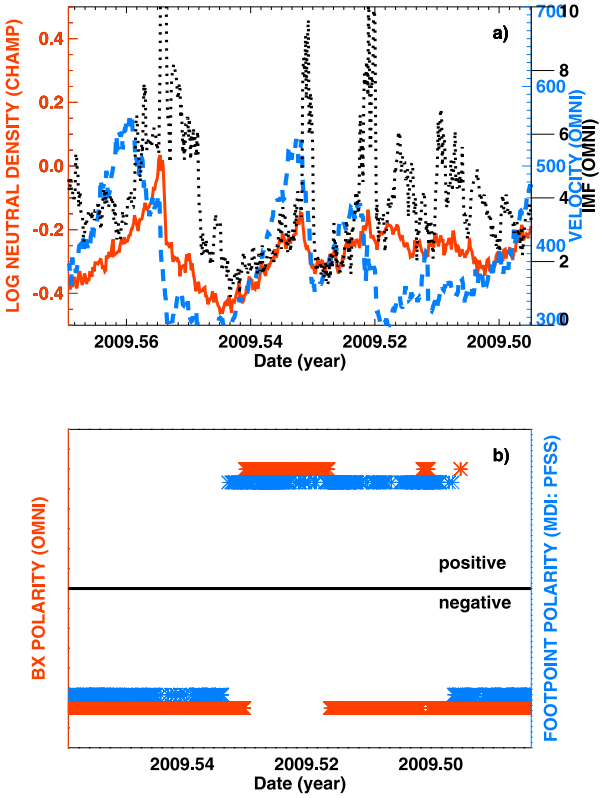


**Figure 12** WHI 3 (CR 2085: 26 June – 22 July 2009) time series. (a) (Blue) OMNI solar-wind velocity and (black) interplanetary magnetic field (IMF), and (red) thermospheric neutral density (ascending orbit) from CHAMP satellite ($10^{-12}$ kg m$^{-3}$). Quantities are plotted *vs.* the time they were measured, however, the interval shown is shifted to four days later than the WHI 3 solar interval to account for average solar-wind travel time. Note also that time goes opposite to the direction of longitude, and so has been plotted backward for ease of comparison to Figure 10. (b) (Red asterisks) Polarity of radial (outward from Sun = positive) component of magnetic field determined from OMNI $B_x$ (daily averages). (Blue triangles) Polarity of radial magnetic field at footpoint of Sun–Earth connecting field line (as described in Figure 10). OMNI $B_x$ measurements are plotted *vs.* time of solar-wind origin, assuming travel time based on solar-wind velocity measured *in situ* at the same time as $B_x$. Time goes right to left.

emergence. McIntosh *et al.* (2011b) made a similar argument for the continued decrease of supergranule spatial scale that occurred throughout this minimum, resulting in a smaller size scale for supergranules than measured for previous minima. This ongoing evolution through the minimum implies a gradual decay, unlike the behavior of sunspots or for that matter granulation and the photospheric network (Muller, Utz, and Hanslmeier, 2011), which were largely unchanged during this period.

Another class of solar observations that demonstrated evolution during the time period 2008 – 2010 were helioseismic oscillations. The frequencies of these modes are sensitive to the conditions in the interior of the Sun and also to the thermodynamic and magnetic environment around their upper turning point at the solar photosphere. Tripathy *et al.* (2010) analyzed modes that sense the outer 30% in radius. They pointed out that these intermediate-degree frequency shifts, which vary in phase with the 11-year sunspot cycle, continued to

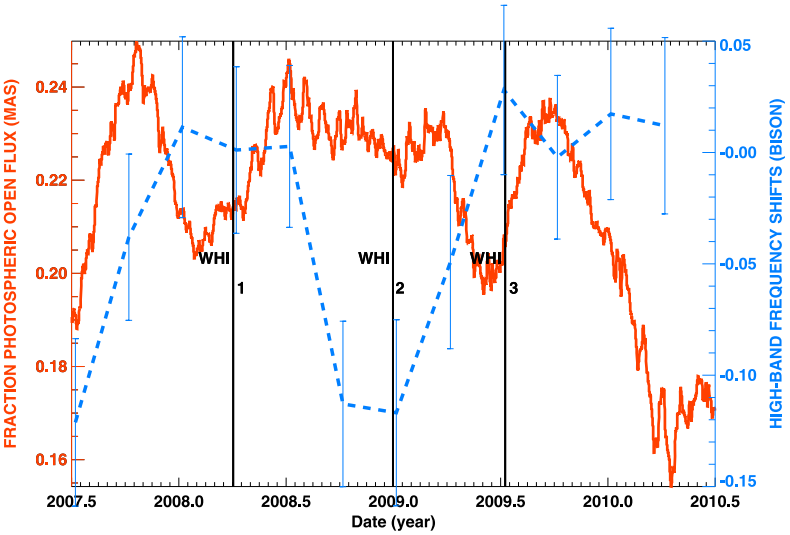


**Figure 13** Quantities showing quasi-biennial modulation during minimum. (Red) Total coronal-hole area obtained from MAS open-field footpoints (three-rotation running average). (Blue) BiSON $\ell = 0, 1, 2$ modes in high-frequency band shifts (microhertz) (*e.g.* Fletcher *et al.*, 2010) (91.25-day average required to obtain sufficient signal to noise). Errors are from formal errors and the fitting.

decrease through September 2009. Thus, like the supergranules and visible–infrared solar radiation, a gradual evolution continued.

The Birmingham Solar Oscillations Network (BiSON) data are sensitive to the low-degree modes that probe most of the volume of the Sun. Fletcher *et al.* (2010) reported an interesting quasi-biennial oscillation (QBO) in the frequency shifts, seen alongside the 11-year variation. This shorter-term variation is modulated by the longer cycle and continues into the solar minimum (Figure 13 blue). The radial-mode frequency dependence of this QBO is less marked than that of the 11-year variation and this indicates that a larger radial extent of the upper atmosphere of the Sun is involved in the QBO modulation than in the 11-year modulation. Fletcher *et al.* (2010) consequently argued that the QBO was evidence of a local dynamo operating in the upper 5% of the solar interior, acting as a modulator of the 11-year cycle flux emerging from deeper within the Sun's interior.

Observations of photospheric magnetic fields, sunspots, and flares during solar maximum have previously been used as evidence for a quasi-biennial modulation, and with it, a local dynamo (Benevolenskaya, 1998a, 1998b). During solar minimum, such indicators associated with flux emergence are weak or non-existent, and no meaningful modulation can be found. However, coronal holes evolve as a consequence of flux emergence. We therefore have plotted the total coronal-hole area as measured from the MAS open-field footpoints in Figure 13 (red). A QBO is arguably present in both the coronal-hole area and the BiSON frequency shifts, but with a phase shift (indeed the two quantities appear nearly anti-correlated). It is possible that the frequency shifts are responding to the changes at their upper boundary as the open flux evolves. Alternatively, the two quantities (mode shifts and open flux) may not be directly related, but rather may both be responding in some way to the modulation of a local dynamo.

## 4.2. The Heliosphere at Its Quietest

### *4.2.1. Transient Disturbances*

As discussed above, flux emergence, irradiance, and activity reached low levels in 2008 and stayed low. Over the course of the next year and a half, the open flux evolved as described above and lost the long-lived and localized open-flux regions that had caused recurring HSS. In 2008 there was a bimodal distribution of solar-wind speed at the Earth because of the prevalence of those HSS. In 2009 this bimodal distribution was gone, and the Earth sat mostly in slow wind (de Toma, 2011).

While faster-wind streams still occurred in 2009, their amplitude was low. In 1997 the amplitudes of fast streams reached similarly low levels, but at a time when new-cycle flux was already on the uprise at the Sun and with it interplanetary CMEs (ICMEs) and the IMF (*e.g.* Jian, Russell, and Luhmann, 2011). Although the number of CMEs did increase in 2009, ICMEs measured *in situ* were shorter in duration and weaker in magnetic field and dynamic pressure than at last minimum (Lepping *et al.*, 2011). Weak dynamic pressure and slower fast magnetosonic speed for this minimum also meant that although there were more interplanetary shocks, they were weaker (see also Jackman and Arridge, 2011). Thus, the heliosphere was largely unperturbed by transient disturbances.

### *4.2.2. Geospace and the Earth's Upper Atmosphere*

The weakness of the solar wind was reflected in the weakness of the Earth's radiation belt, which decreased in late 2009 to levels lower than ever measured in the space age (Russell, Luhmann, and Jian, 2010). Thermospheric neutral density was similarly low. Indeed, satellite-drag measurements indicate that thermospheric densities reached lower levels than previously seen (Emmert, Lean, and Picone, 2010; Solomon *et al.*, 2010). Ionospheric vertical total electron content also showed a decrease relative to the last minimum, although the difference was small, and NmF2 (peak concentration in F region) showed a less clear behavior (in some instances it was higher than the previous minimum) (Araujo Pradere *et al.*, 2011). $F_{10.7}$ flux was lower for this minimum than the last, as was even more dramatically the case for EUV radiation. The low EUV radiation may be the cause of the decrease in thermospheric densities (Solomon *et al.*, 2011). Whether or not total solar irradiance was lower for this minimum is still being debated (Fröhlich, 2009; Haberreiter, 2011; Kopp and Lean, 2011).

### *4.2.3. Heliospheric Magnetic Flux*

The IMF reached very low levels by 2009 (approximately 3 nT), lower than measured in prior minima (Emery *et al.*, 2011). This forced a revision of what had been previously thought of as an absolute lower limit, or "floor" in heliospheric magnetic field (Svalgaard and Cliver, 2007). The reason for the decrease for this minimum was argued to be either there being less input from ICMEs (Owens *et al.*, 2008) or a weaker input from solar polar magnetic flux (Cliver and Ling, 2011). Alternatively, Zhao and Fisk (2011) argued that actually the flux was the same between the two minima, but that the field strength was lower for this minimum because it filled a larger area as a consequence of narrower streamer stalks (see discussion above).

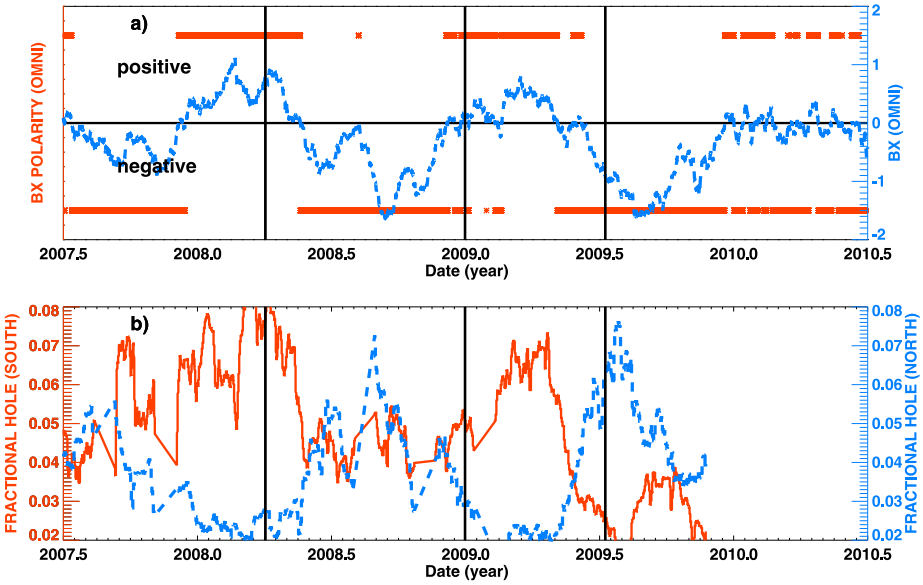


**Figure 14** (a) 27-day running average of (red) polarity of radial component of magnetic field determined from OMNI $B_x$ and (blue) OMNI $B_x$ (nanotesla); positive is radially outward, negative is radially inward to Sun. (b) Fractional coronal-hole area (averaged over each Carrington rotation) for (red) southern hemisphere and (blue) northern hemisphere, determined from coronal holes mapped from observations as in de Toma (2011). Solar B-angle semi-annual variation is clearly seen in both. Vertical lines show the centers of WHI 1 – WHI 3.

### *4.2.4. Cosmic Rays*

Galactic cosmic rays reached a space-age maximum in late 2009. This ultimate limit was reached because of a combination of factors, including weaker and less-turbulent IMF, slower solar-wind speed, and lower dynamic pressure than measured in prior minima; of these, the best correlation was with the decrease in IMF (Mewaldt *et al.*, 2010). The HCS was not as flat as during prior minima, but the open magnetic flux was generally incoherent and "porcupiney," which may also have acted to promote the ingress of galactic cosmic rays (McIntosh *et al.*, 2011a). We note that the climb to unprecedented cosmic-ray levels occurred as coronal holes (open magnetic-flux regions) lost coherence and periodicity.

### *4.2.5. Northern vs. Southern Hemisphere Connectivity*

The Earth is at maximum southern heliolatitudes annually in March, with maximum northern heliolatitudes reached in September and near-equatorial latitudes reached in December and June. If the HCS is not very tilted, the northern hemisphere is predominantly of one sign (negative this most recent minimum) and the southern hemisphere of the other (positive this most recent minimum). Consequently, if solar activity is low, a semi-annual variation in the polarity of the radial (outward from Sun) field becomes apparent (Emery *et al.*, 2011; Jian, Russell, and Luhmann, 2011). Figure 14(a) shows the solar-wind magnetic-field direction measured *in situ*. The semi-annual variation is clear until 2010, as seen both in the polarity (red dots) which changes sign in Spring and Fall, and in the sinusoidal variation of the field-line direction (blue). Figure 14(b) plots the fractional coronal-hole area for North

*vs.* South as determined from solar observations (de Toma, 2011). Because of the Earth's varying heliolatitude, northern- and southern-polar coronal holes (which constitute the majority of the fractional area shown) alternate in dominance.

There is a notable offset from zero (horizontal line) in Figure 14(a) so that there is more negative polarity overall. This is consistent with a southward shift of the HCS, which has been noted for the past few solar cycles (Mursula and Virtanen, 2011; Wang and Robbrecht, 2011), as a consequence of which the low-latitude northern polarity originates in the southern hemisphere. Thus some of the southern coronal-hole area shown in Figure 14(b), especially near the Equator, is likely to have northern (negative) polarity. WHI 1 illustrates an example of this: the near-equatorial coronal hole around 275° has northern (negative) polarity, but, because of the dip in the HCS, the field lines that intersect the Earth are rooted in the southern hemisphere.

## 5. Conclusions

In conclusion, two aspects of the recent minimum were at the heart of its "peculiarity": Solar polar magnetic fields were weak, and new-cycle flux emergence was slow to start.

The weak polar fields resulted in a complex coronal magnetic-field morphology, including low- and mid-latitude coronal holes and pseudo-streamers that persisted throughout the minimum. The Sun never did become a classic solar minimum dipole, even though the HCS eventually flattened. In the early stages of the minimum, the pronounced longitudinal asymmetry resulted in periodic forcing of the heliosphere and Earth by HSSs. Declining-phase behavior persisted but on a background of excessively low solar irradiance and activity. WHI 1 was a good example of this, and continues to be an excellent focus period for tuning models on a system where the effects of periodic solar-wind forcing of the Earth's environment occur in an otherwise unperturbed background (*e.g.* Wang *et al.*, 2011).

The delay in new-cycle flux emergence resulted in a long period in which the heliosphere could evolve toward a ground state. A lag in minimum for heliospheric and geospace quantities is not unusual. Because of the extended period of low activity and the generally weak solar output, however, the heliosphere reached a baseline solar minimum configuration unique in the Space Age. IMF, cosmic rays, and radiation belts all reached record levels as the open flux evolved to an axisymmetric, but porcupine-like distribution. At the Sun, magnetic flux continued to be churned to smaller and smaller spatial scales, and the minimum was long enough and quiet enough for a quasi-biennial modulation to have been apparent in helioseismic modes.

The solar minimum did, by any definition, finally end and Cycle 24 began. Flux emergence rose sharply in late 2009, and the heliosphere and terrestrial environment responded quickly. It did not turn out to be a "grand minimum" as some at first suggested it might, but it remains a remarkably interesting one, nonetheless.



**Acknowledgements** We thank Todd Hoeksema, Marc DeRosa, Alysha Reinard, and Larisza Krista for useful discussions. The hourly solar-wind plasma and IMF data were taken from the OMNI-2 collection from the Space Physics Data Facility at the Goddard Space Flight Center managed by Natalia Papitashvili. This study used indices from the CEDAR Database at the National Center for Atmospheric Research (NCAR), which is supported by the National Science Foundation. J. Lei thanks Eric Sutton for providing CHAMP data and support from the 100 Talents Program of the Chinese Academy of Science. SOHO is a project of

international collaboration between ESA and NASA. We gratefully acknowledge the use of the SolarSoft package for generating PFSS fields developed by Marc DeRosa. Radiation-belt electron-number fluxes from the GOES satellites come from NGDC via SPIDR at http://spidr.ngdc.noaa.gov starting with GOES-05 in January 1986 and extending through GOES-12. We thank Terry Onsager for his comments and assistance with these data. We also thank Anne-Marie Broomhall for assistance with the BiSON data, and Thomas Kuchar for assistance with the CACTus CME data. The research of L. Zhao is supported by the NASA Living with a Star Heliophysics Postdoctoral Fellowship Program, administered by the University Corporation for Atmospheric Research.

## References

Abramenko, V., Yurchyshyn, V., Linker, J., Mikic, Z., Luhmann, J., Lee, C.: 2010, Low-latitude coronal holes at the minimum of the 23rd solar cycle. *Astrophys. J.* **712**, 813.

Araujo Pradere, E.A., Redmon, R., Fedrizzi, M., Viereck, R., Fuller-Rowell, T.J.: 2011, Some characteristics of the ionospheric behavior during the solar cycle 23 – 24 minimum. *Solar Phys.* doi:10.1007/s11207-011-9728-3.

Arge, C.N., Pizzo, V.J.: 2000, Improvement in the prediction of solar wind conditions using near-real time solar magnetic field updates. *J. Geophys. Res.* **105**, 10465.

Aschwanden, M.J.: 2011, The state of self-organized criticality of the sun during the last three solar cycles. I. Observations. *Solar Phys.* doi:10.1007/s11207-011-9755-0.

Benevolenskaya, E.E.: 1998a, Longitudinal structure of the double magnetic cycle. *Solar Phys.* **181**, 479.

Benevolenskaya, E.E.: 1998b, A model of the double magnetic cycle of the Sun. *Astrophys. J. Lett.* **509**, L49.

Chamberlin, P.C., Woods, T.N., Crotser, D.A., Eparvier, F.G., Hock, R.A., Woodraska, D.L.: 2009, Solar cycle minimum measurements of the solar extreme ultraviolet spectral irradiance on 14 April 2008. *Geophys. Res. Lett.* **36**, L05102. doi:10.1029/2008GL037145.

Cliver, E.W., Ling, A.G.: 2011, The floor in the solar wind magnetic field revisited. *Solar Phys.* doi:10.1007/s11207-010-9657-6.

Cremades, H., Mandrini, C.H., Dasso, S.: 2011, Coronal transient events during two solar minima: their solar source regions and their interplanetary consequences. *Solar Phys.* doi:10.1007/s11207-011-9769-7.

de Toma, G.: 2011, Evolution of coronal holes and implications for high-speed solar wind during the minimum between cycles 23 and 24. *Solar Phys.* doi:10.1007/s11207-010-9677-2.

Echer, E., Tsurutani, B.T., Gonzalez, W.D., Kozyra, J.U.: 2011, High speed stream properties and related geomagnetic activity during the whole heliosphere interval (WHI): 20 March to 16 April 2008. *Solar Phys.* doi:10.1007/s11207-011-9739-0.

Emery, B.A., Richardson, I.G., Evans, D.S., Rich, F.J., Wilson, G.R.: 2011, Solar rotational periodicities and the semiannual variation in the solar wind, radiation belt, and aurora. *Solar Phys.* doi:10.1007/s11207-011-9758-x.

Emmert, J.T., Lean, J.L., Picone, J.M.: 2010, Anomalously low solar extreme-ultraviolet irradiance and thermospheric density during solar minimum. *Geophys. Res. Lett.* **37**, L12102. doi:10.1029/2010GL043671.

Fletcher, S.T., Broomhall, A.-M., Salabert, D., Basu, S., Chaplin, W.J., Elsworth, Y., Garcia, R.A., New, R.: 2010, A seismic signature of a second dynamo? *Astrophys. J. Lett.* **718**, L19.

Fröhlich, C.: 2009, Evidence of a long-term trend in total solar irradiance. *Astron. Astrophys.* **501**, 27.

Gibson, S.E., Kozyra, J.U., de Toma, G., Emery, B.A., Onsager, T., Thompson, B.J.: 2009, If the sun is so quiet, why is the earth still ringing? a comparison of two solar minimum intervals. *J. Geophys. Res.* **114**, A09105. doi:10.1029/2009JA014342.

Haberreiter, M.: 2011, Solar EUV spectrum calculated for quiet sun conditions. *Solar Phys.* doi:10.1007/s11207-011-9767-9.

Hundhausen, A.J.: 1972, *Coronal Expansion and Solar Wind*, Springer, Berlin.

Jackman, C.M., Arridge, C.S.: 2011, Solar cycle effects on the dynamics of Jupiter's and Saturn's magnetospheres. *Solar Phys.* doi:10.1007/s11207-011-9748-z.

Jian, L.K., Russell, C.T., Luhmann, J.G.: 2011, Comparing solar minimum 23/24 with historical solar wind records at 1 AU. *Solar Phys.* doi:10.1007/s11207-011-9737-2.

Judge, P.G., Burkepile, J., de Toma, G., Druckmueller, M.: 2010, In: Cranmer, S.R., Hoeksema, J.T., Kohl, J.L. (eds.) *Historical eclipses and the recent solar minimum compared. SOHO-23: Understanding a Peculiar Solar Minimum* **CS-428**, Astron. Soc. Pacific, San Francisco, 171.

Kirk, M.S., Pesnell, W.D., Young, C.A., Hess Webber, S.A.: 2009, Automated detection of EUV polar coronal holes during solar cycle 23. *Solar Phys.* **257**, 99. doi:10.1007/s11207-009-9369-y.

Kopp, G., Lean, J.L.: 2011, A new, lower value of total solar irradiance: evidence and climate significance. *Geophys. Res. Lett.* **38**, L01706. doi:10.1029/2010GL045777.

Leamon, R.J., McIntosh, S.W.: 2009, How the solar wind ties to its photospheric origins. *Astrophys. J. Lett.* **697**, L28.
Lee, C.O., Luhmann, J.G., Hoeksema, J.T., Arge, C.N., de Pater, I.: 2011, Coronal field opens at lower height during the solar cycles 22 and 23 minimum periods: IMF comparison suggests the source surface should be lowered. *Solar Phys.* **269**, 367. doi:10.1007/s11207-010-9699-9.
Lei, J., Thayer, J.P., Wang, W., McPherron, R.L.: 2011, Impact of cir storms on thermosphere density variability during the solar minimum of 2008. *Solar Phys.* doi:10.1007/s11207-010-9563-y.
Lepping, R.P., Wu, C.-C., Berdichevsky, D.B., Szabo, A.: 2011, Magnetic clouds at/near the 2007–2009 solar minimum: frequency of occurrence and some unusual properties. *Solar Phys.* doi:10.1007/s11207-010-9646-9.
McIntosh, S.W., Burkepile, J., Gurman, J.B., Leamon, R.J., Olive, J.-P.: 2011a, The highest cosmic rays ever recorded: what happened to the Earth's deflector shield? *Astrophys. J. Lett.* in press.
McIntosh, S.W., Leamon, R.J., Hock, R.A., Rast, M.P., Ulrich, R.K.: 2011b, Observing evolution of the supergranular network length scale during periods of low solar activity. *Astrophys. J. Lett.* **660**, L1653.
Mewaldt, R.A., Davis, A.J., Lave, K.A., Leske, R.A., Stone, E.C., Wiedenbeck, M.E., Bins, W.R., Christian, E.R., Cummings, A.C., de Nolfo, G.A., Israel, M.H., Labrador, A.W., von Rosenvinge, T.T.: 2010, Record-setting cosmic-ray intensities in 2009 and 2010. *Astrophys. J. Lett.* **723**, L1.
Muller, R., Utz, D., Hanslmeier, A.: 2011, Non-varying granulation and photospheric network during the extended 2007–2009 solar minimum. *Solar Phys.* doi:10.1007/s11207-011-9725-6.
Mursula, K., Virtanen, I.: 2011, The last dance of the bashful ballerina? *Astron. Astrophys. Lett.* **525**, 12. doi:10.1051/0004-6361/200913975.
Nitta, N.V.: 2011, Observables indicating two major coronal mass ejections during the WHI. *Solar Phys.* doi:10.1007/s11207-011-9806-6.
Owens, M.J., Crooker, N.U., Schwadron, N.A., Horbury, T.S., Yashiro, S., Xie, H., St. Cyr, O.C., Gopalswamy, N.: 2008, Conservation of solar magnetic flux and the floor in the heliospheric magnetic field. *Geophys. Res. Lett.* **35**, 20108. doi:10.1029/2008GL035813.
Petrie, G.J.D., Canou, A., Amari, T.: 2011, Nonlinear force-free and potential-field models of active-region and global coronal fields during the whole heliosphere interval. *Solar Phys.* doi:10.1007/s11207-010-9687-0.
Poduval, B., Zhao, X.-P.: 2004, Discrepancies in the prediction of solar wind using potential field source surface model: An investigation of possible sources. *J. Geophys. Res.* **109**, A08102. doi:10.1029/2004JA010384.
Riley, P., Luhmann, J.: 2011, Interplanetary signatures of unipolar streamers and the origin of the slow solar wind. *Solar Phys.* doi:10.1007/s11207-011-9909-0.
Riley, P., Lionello, R., Linker, J.A., Mikic, Z., Luhmann, J., Wijaya, J.: 2011, Global MHD modeling of the solar corona and inner heliosphere for the whole heliosphere interval. *Solar Phys.* doi:10.1007/s11207-010-9698-x.
Russell, C.T., Luhmann, J.G., Jian, L.K.: 2010, How unprecedented a solar minimum? *Geophys. Res. Lett.* **48**, RG2004. doi:10.1029/2009RG000316.
Schrijver, C., DeRosa, M.: 2003, Photospheric and heliospheric magnetic fields. *Solar Phys.* **212**, 165.
Sheeley, J.N.R.: 2008, A century of polar faculae variations. *Astrophys. J.* **680**, 1553.
Smith, E.J., Balogh, A.: 2008, Decrease in heliospheric magnetic flux in this solar minimum: Recent Ulysses magnetic field observations. *Geophys. Res. Lett.* **35**, L22103. doi:10.1029/2008GL035345.
Solomon, S.C., Woods, T.N., Didkovsky, L.V., Emmert, J.T., Qian, L.: 2010, Anomalously low solar extreme-ultraviolet irradiance and thermospheric density during solar minimum. *Geophys. Res. Lett.* **37**, L16103. doi:10.1029/2010GL044468.
Solomon, S.C., Qian, L., Didkovsky, L.V., Viereck, R.A., Woods, T.N.: 2011, Causes of low thermospheric density during the 2007–2009 solar minimum. *J. Geophys. Res.* **116**, A00H07. doi:10.1029/2011JA016508.
Svalgaard, L., Cliver, E.W.: 2007, A floor in the solar wind magnetic field. *Astrophys. J. Lett.* **661**, L203.
Thompson, B.J., Gibson, S.E., Schroeder, P.C., Webb, D.F., Arge, C.N., Bisi, M.M., de Toma, G., Emery, B.A., Galvin, A.B., Haber, D.A., Jackson, B.V., Jensen, E.A., Leamon, R.J., Lei, J., Manoharan, P.K., Mays, M.L., McIntosh, P.S., Petrie, G.J.D., Plunkett, S.P., Qian, L., Riley, P., Suess, S.T., Tokumaru, M., Welsch, B.T., Woods, T.N.: 2011, A snapshot of the Sun near solar minimum: the whole heliosphere interval. *Solar Phys.* doi:10.1007/s11207-011-9891-6.
Tokumaru, M., Kojima, M., Fujiki, K., Hayashi, K.: 2009, Non-dipolar solar wind structure observed in the cycle 23/24 minimum. *Geophys. Res. Lett.* **36**, L09101. doi:10.1029/2009GL037461.
Tripathy, S.C., Jain, K., Hill, F., Leibacher, J.W.: 2010, Unusual trends in solar p-mode frequencies during the current extended minimum. *Astrophys. J. Lett.* **711**, L84.
Tsurutani, B.T., Echer, E., Gonzalez, W.D.: 2011, The solar and interplanetary causes of the recent minimum in geomagnetic activity (mga23): a combination of midlatitude small coronal holes, low IMF bz variances, low solar wind speeds and low solar magnetic fields. *Ann. Geophys.* **29**, 1.

Vasquez, A., Huang, Z., Manchester, W.B., Frazin, R.A.: 2011, The WHI corona from differential emission measure tomography. *Solar Phys.* doi:10.1007/s11207-010-9706-1.

Vourlidas, A., Howard, R.A., Esfandiari, E., Patsourakos, S., Yashiro, S., Michalek, G.: 2010, Comprehensive analysis of coronal mass ejection mass and energy properties over a full solar cycle. *Astrophys. J.* **722**, 1522.

Wang, Y.-M., Robbrecht, E.: 2011, Asymmetric sunspot activity and the southward displacement of the current sheet. *Astrophys. J.* **736**, 136.

Wang, Y.-M., Sheeley, N.R.J., Rich, N.B.: 2007, Coronal pseudostreamers. *Astrophys. J.* **658**, 1340.

Wang, W., Lei, J., Burns, A.G., Qian, L., Solomon, S.C., Wiltberger, M., Xu, J.: 2011, Ionospheric day-to-day variability around the whole heliosphere interval in 2008. *Solar Phys.* doi:10.1007/s11207-011-9747-0.

Webb, D.F., Cremades, H., Sterling, A.C., Mandrini, C.H., Dasso, S., Gibson, S.E., Haber, D.A., Komm, R.W., Petrie, G.J.D., McIntosh, P.S., Welsch, B.T., Plunkett, S.P.: 2011, The global context of solar activity during the whole heliosphere interval campaign. *Solar Phys.* doi:10.1007/s11207-011-9787-5.

Welsch, B., Christe, S., McTiernan, J.M.: 2011, Photospheric magnetic evolution in the WHI active regions. *Solar Phys.* doi:10.1007/s11207-011-9759-9.

White, O., Kopp, G., Snow, M., Tapping, K.: 2011, The solar cycle 23 – 24 minimum. *Solar Phys.* doi:10.1007/s11207-010-9680-7.

Woods, T.N., Chamberlin, P.C., Harder, J.W., Hock, R.A., Snow, M., Eparvier, F.G., Fontenla, J., McClintock, W.E., Richard, E.C.: 2009, Solar irradiance reference spectra (SIRS) for the 2008 whole heliosphere interval (WHI). *Geophys. Res. Lett.* **36**, L01101. doi:10.1029/2008GL036373.

Zhao, L., Fisk, L.: 2011, Understanding the behavior of the heliospheric magnetic field and the solar wind during the unusual solar minimum between cycles 23 and 24. *Solar Phys.* doi:10.1007/s11207-011-9840-4.

Zhao, X.P., Webb, D.F.: 2002, Source regions and storm effectiveness of frontside full halo coronal mass ejections. *J. Geophys. Res.* **108**, 1234. doi:10.1029/2002JA009606.